University of Northern Colorado
Scholarship & Creative Works @ Digital UNC

Undergraduate Honors Theses | Student Work

5-1-2024

Geometric Identification of Discrete Painlevé Equations

Logan Moore
University of Northern Colorado

Follow this and additional works at: https://digscholarship.unco.edu/honors

Recommended Citation

Moore, Logan, "Geometric Identification of Discrete Painlevé Equations" (2024). *Undergraduate Honors Theses*. 96.
https://digscholarship.unco.edu/honors/96

This Thesis is brought to you for free and open access by the Student Work at Scholarship & Creative Works @ Digital UNC. It has been accepted for inclusion in Undergraduate Honors Theses by an authorized administrator of Scholarship & Creative Works @ Digital UNC. For more information, please contact Nicole.Webber@unco.edu.

University of Northern Colorado
Greeley, Colorado

GEOMETRIC IDENTIFICATION OF DISCRETE PAINLEVÉ EQUATIONS

A Capstone
Submitted in Partial
Fulfillment for Graduation with Honors Distinction and
the Degree of Bachelor of Science

Logan Moore

College of Natural and Health Sciences

May 2024

GEOMETRIC IDENTIFICATION OF DISCRETE PAINLEVÉ EQUATIONS

PREPARED BY:

APPROVED BY
CAPSTONE ADVISOR:

HONORS
CHAIR:

HONORS
EXECUTIVE DIRECTOR:

RECEIVED BY THE UNIVERSITY CAPSTONE
PROJECT COMMITTEE ON:

05 / 04 / 2024

Abstract

This thesis determines the type of a particular discrete Painlevé equation using a geometric approach based on Sakai theory. Previous work on discrete Painlevé equations has connected the dynamics of these equations to actions of their symmetry groups on certain families of rational algebraic surfaces. There is a known procedure for identifying the geometry of a discrete Painlevé equation from its birational mapping. This thesis uses this known procedure to determine the type of a particular discrete Painlevé equation appearing in [9].

Acknowledgements

First and foremost, I would like to thank my thesis advisor, Dr. Anton Dzhamay, for his incredible support and patience throughout my entire research process. I truly could not have completed this project without his guidance and communication, despite us being on opposite sides of the globe for much of it. He pushed me to be the best mathematician I could, and I will be forever grateful for the opportunity to work with him.

I would also like to thank the other mathematics faculty at the University of Northern Colorado, particularly Dr. Nathaniel Eldredge, Dr. Katie Morrison, and Dr. Oscar Levin. These professors helped me cultivate the mathematical understanding necessary for this thesis, and they all offered invaluable advice throughout this project.

In addition, I would like to thank the Honors faculty at the University of Northern Colorado, namely Prof. Annie Epperson and Dr. Corrine Wieben. The honors department helped me turn my pages of mathematical scratch work into a presentable final paper, and I am incredibly grateful for their support.

Finally, I would like to thank my friends, my family, and my wonderful partner. I am stupendously lucky to have a support structure to listen to both my failures and successes (though I imagine they got quite tired of listening by the end). I could not have completed this project without their support.

Table of Contents

Title Page . . . .

Signature Page . . . .

Abstract **1**

Acknowledgements **2**

List of Figures **4**

1 Introduction **5**

2 Method **8**

3 Understanding the Geometry **9**

4 The Applied Example **12**

5 Determining the Surface $\mathcal{X}$ and its Type **13**

6 Identifying the Surface Type and Induced Dynamics on the Picard Lattice **15**

7 Comparing the Dynamics and Determining the Final Change of Basis . **18**

8 Determining the Change of Coordinates **25**

9 Conclusion **30**

References **30**

List of Figures

1 Painlevé Equations $\mathrm{P_I} \ldots \mathrm{P_{VI}}$ 5

2 Sakai's Scheme 7

3 Charts Covering $\mathbb{P}^1 \times \mathbb{P}^1$. 10

4 Visualization of the Blow-Up Procedure. 11

5 The Base Point Configuration and Visualization of the Surface $\mathcal{X}$. 14

6 The Surface Root Dynkin Diagram 15

7 The Symmetry Root Dynkin Diagram 19

8 Generators of $\widetilde{W}\left(A_2^{(1)}\right)$ 20

9 The Point Configuration for the Standard $A_2^{(1)}/E_6^{(1)}$ Example 25

1 Introduction

Painlevé equations are an important family of nonlinear differential equations that were first described by P. Painlevé in 1902 [18]. Painlevé was studying nonlinear ordinary differential equations in search of purely nonlinear special functions. By studying the case where the only movable singularities are poles (now called the Painlevé property), Painlevé and his student B. Gambier found six new families of equations, called Painleve equations $\mathrm{P_I} \ldots \mathrm{P_{VI}}$ (see Figure 1). The solutions to these equations, Painlevé transcendents, are nonlinear special functions that are increasingly important in a wide range of applications.

$$(\mathrm{P_I}) \quad \frac{d^2y}{dt^2} = 6y^2 + t;$$

$$(\mathrm{P_{II}}) \quad \frac{d^2y}{dt^2} = 2y^3 + ty + \alpha;$$

$$(\mathrm{P_{III}}) \quad \frac{d^2y}{dt^2} = \frac{1}{y}\left(\frac{dy}{dt}\right)^2 - \frac{1}{t}\frac{dy}{dt} + \frac{1}{t}(\alpha y^2 + \beta) + \gamma y^3 + \frac{\delta}{y};$$

$$(\mathrm{P_{IV}}) \quad \frac{d^2y}{dt^2} = \frac{1}{2y}\left(\frac{dy}{dt}\right)^2 + \frac{3}{2}y^3 + 4ty^2 + 2(t^2 - \alpha)y + \frac{\beta}{y};$$

$$(\mathrm{P_V}) \quad \frac{d^2y}{dt^2} = \left(\frac{1}{2y} + \frac{1}{y-1}\right)\left(\frac{dy}{dt}\right)^2 - \frac{1}{t}\frac{dy}{dt} + \frac{(y-1)^2}{t^2}\left(\alpha y + \frac{\beta}{y}\right) + \gamma\frac{y}{t} + \delta\frac{y(y+1)}{y-1};$$

$$(\mathrm{P_{VI}}) \quad \frac{d^2y}{dt^2} = \frac{1}{2}\left(\frac{1}{y} + \frac{1}{y-1} + \frac{1}{y-t}\right)\left(\frac{dy}{dt}\right)^2 - \left(\frac{1}{t} + \frac{1}{t-1} + \frac{1}{y-t}\right)\frac{dy}{dt} + \frac{y(y-1)(y-t)}{t^2(t-1)^2}\left(\alpha + \beta\frac{t}{y^2} + \gamma\frac{t-1}{(y-1)^2} + \delta\frac{t(t-1)}{(y-t)^2}\right).$$

Figure 1: Painlevé Equations $\mathrm{P_I} \ldots \mathrm{P_{VI}}$

In contrast, discrete Painlevé equations are a much more recent object of study. These equations were originally defined as second-order nonlinear recurrence relations that became a differential Painlevé equation in a continuous limit. The first discrete Painlevé equation was explicitly identified in 1990, coming from the study of quantum gravity [6]. In the coming decades, mathematicians obtained many examples of discrete Painlevé equations via several approaches, such as applying the singularity confinement criterion to deautonomizations of

QRT maps [8]. However, at the time, there was no clear understanding of the nature of discrete Painlevé equations. Instead, there was a large collection of various examples whose labeling in terms of continuous limits became increasingly convoluted.

It would take another decade for the appropriate definition and classification scheme to emerge. In 2001, H. Sakai published his seminal paper on the geometric theory of Painlevé equations [12]. Using techniques from algebraic geometry, Sakai defined discrete Painlevé equations in terms of actions of an affine Weyl group on a certain family of rational algebraic surfaces. This introduced a new way of classifying the discrete Painlevé equations, one based on their associated rational surfaces, of which there are 22 different types (see Figure 2). Since then, Sakai theory has reached a relatively mature state. For more information on the history of discrete Painlevé equations, refer to [8] and [15].

Unfortunately, Sakai theory has a high barrier to entry. Fully understanding the scheme requires significant knowledge of several domains of mathematics, such as algebraic geometry and representation theory. Notably, though, the Painlevé equations are of interest in applications. For example, the discrete Painlevé equations have applications to studying random matrices and orthogonal polynomials (see [14], [19], [20], [2], and [13]). Thus, it is important for applied mathematicians to recognize and describe discrete Painlevé equations when they encounter them, making the high barrier to entry concerning.

The project that I'm working on is to catalogue various examples of discrete Painlevé equations that were discovered in applications and labelled by their continuous limits in terms of the algebro-geometric data of Sakai theory. Namely, starting from a second-order nonlinear recurrence relation, we resolve its singularity structure to make it a well-defined discrete dynamic on one of the families of Sakai surfaces characterized by a translation element in the affine Weyl symmetry group of the family. Such a procedure was carefully described in [4]. In this paper, we focus on one particular example of such an identification. We study a recurrence relation obtained in a recent paper, [9], by Min and Wang, who

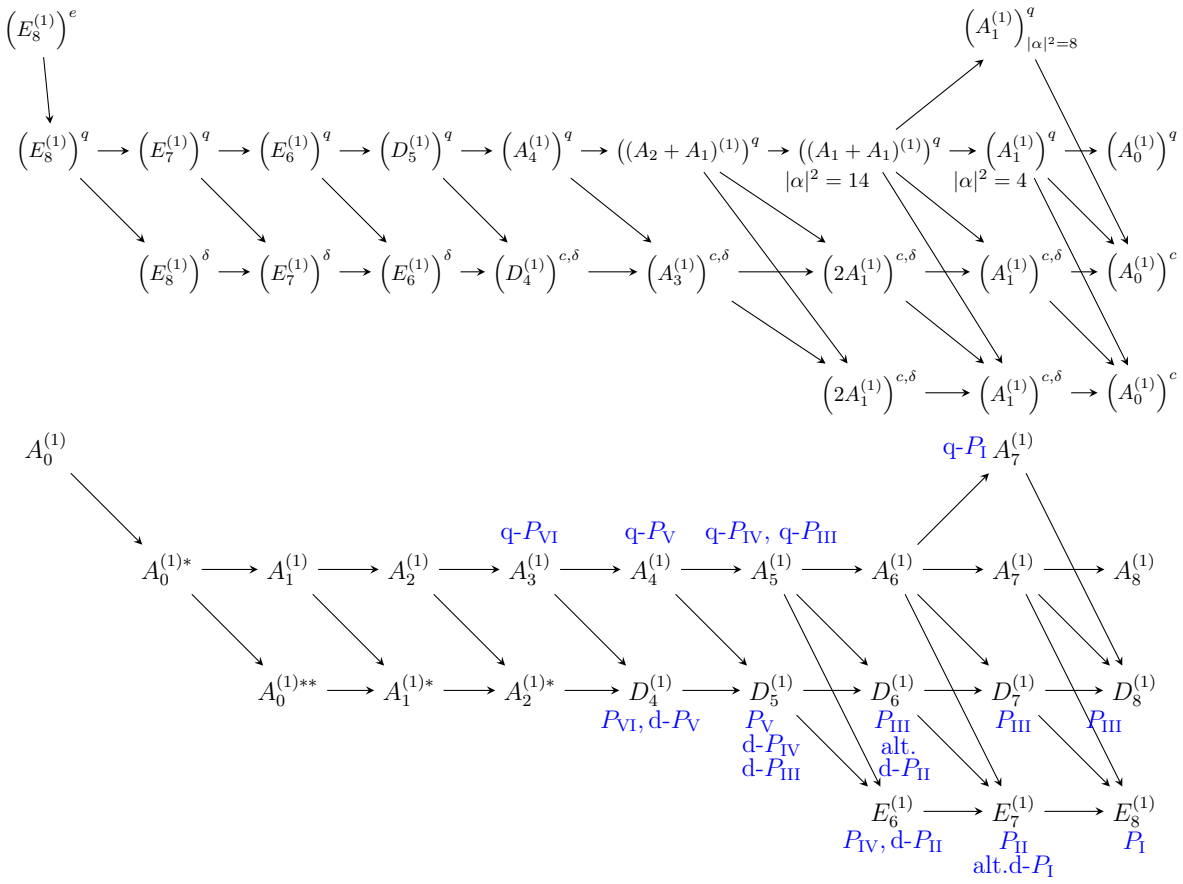

Figure 2: Sakai's Scheme: Surface Type (above) and Symmetry Type (below). Image adapted from Anton Dzhamay, used with permission.

studied orthogonal polynomials for a Gaussian weight with a jump.

2 Method

In this section, we give a very brief outline of the known identification procedure. Later, we explain this process in detail. We start with a recurrence relation in two variables. Using this, we can define rational maps of the complex plane to itself for each variable. Next, we compactify our space from $\mathbb{C} \times \mathbb{C}$ to $\mathbb{P}^1 \times \mathbb{P}^1$ by adding points at infinity in each coordinate. Finally, we resolve the indeterminacies of our map, for which we expect to find eight, using the blow-up procedure from algebraic geometry.

The procedure described in the previous paragraph created a family of rational algebraic surfaces. Associated with this family of surfaces is an algebraic object known as the Picard lattice, which can be used to study the dynamic of our system. The Picard lattice of our family of surfaces contains two important sublattices which can be described by certain graphs, known as Dynkin diagrams. One sublattice characterizes the geometry of our surface family, and its Dynkin diagram defines the surface type of our dynamic. A dual sublattice characterizes the symmetry of our surface family, to which we associate an affine Weyl group, which is a symmetry group of our family. The Dynkin diagram of this sublattice defines the symmetry type of our dynamic.

Our dynamic induces a linear map on the Picard lattice. We then identify this linear map with a translation element of the associated Weyl group. The triple consisting of the surface type, the symmetry type, and the translation element is the abstract characterization of a discrete Painlevé equation in Sakai theory.

The final step is to construct an explicit matching of our dynamic to a dynamic on one of the 22 surface families by finding a change of coordinates. For each surface type, we have some standard examples of equations, usually corresponding to short translation elements.

It often happens that our final change of coordinates reduces our original equation to one of these standard examples. In such cases, we first find a matching of the surface type by constructing a preliminary change of basis between the two Picard lattices. We then identify the dynamic by matching the surface sublattices and computing the associated translation element. If this translation element is different but conjugated with one of the standard examples, then we must adjust our preliminary change of basis by an action of some element of our Weyl group. Finally, we can extend the change of basis on the Picard lattice to an explicit change of coordinates that transforms our discrete Painlevé equation to a standard example.

3 Understanding the Geometry

Discrete Painlevé equations are usually written as maps from $\mathbb{P}^1 \times \mathbb{P}^1$ to itself defined by rational functions that also have rational inverses (such maps are called birational). Here, $\mathbb{P}^1$ is the complex projective line (sometimes called the Riemann sphere), consisting of the complex numbers adjoined with an unsigned point at infinity. To compactify $\mathbb{C} \times \mathbb{C}$ with (x, y) coordinates to $\mathbb{P}^1 \times \mathbb{P}^1$, we introduce new coordinates, $X = 1/x$ and $Y = 1/y$, such that the value $X = 0$ corresponds to the point at infinity in the x coordinate. To cover the entire $\mathbb{P}^1 \times \mathbb{P}^1$ space, we need a total of 4 coordinate charts: (x, y), (X, y), (x, Y), and (X, Y) (see Figure 3).

Since our maps are given by birational functions, the only issues come from "division by zero". An important property of compactifying from $\mathbb{C} \times \mathbb{C}$ to $\mathbb{P}^1 \times \mathbb{P}^1$ is a rigorous way of understanding expressions of the form $\frac{1}{0}$. Namely, dividing any non-zero number by 0 will evaluate to the point at infinity. Thus, when a map produces an expression where only the denominator vanishes, the map will send that point to the zero of the inverse coordinate. However, it is also possible for maps to result in $\frac{0}{0}$ expressions, which are still indeterminate

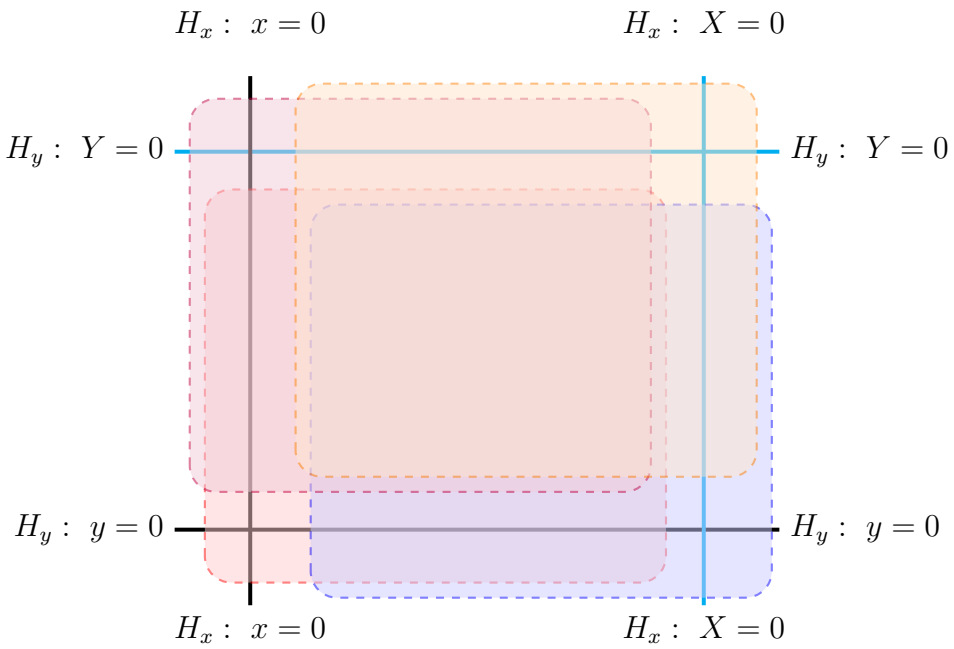

Figure 3: Charts Covering $\mathbb{P}^1 \times \mathbb{P}^1$. Image by Anton Dzhamay, used with permission.

on $\mathbb{P}^1 \times \mathbb{P}^1$. We need to introduce more charts to resolve these.

To construct these new charts, we will use the blow-up procedure from algebraic geometry. The blow-up procedure resolves $\frac{0}{0}$ indeterminacies by "lifting" the lines that pass through the blow-up point and separating them based on their slope. This lifting corresponds to a projection π from the blown-up space to the original space such that π^{-1} is one to one everywhere except the point being blown up, which instead maps to a new projective line $\mathbb{P}^1$ (see Figure 4). This new line is called an exceptional divisor, denoted by E_i or F_i throughout this paper. Note that for any line L containing the blown-up point, $L-E_i$ or $L-F_i$ represents the proper transform under π^{-1}, which is the mapping of every point on the line except the blown-up point.

Algebraically, when we blow up a point $(x = x_0, y = y_0)$, we introduce two new coordinate charts: (u, v) and (U, V). In the (u, v) chart, $u = x - x_0$ and $v = \frac{y-y_0}{x-x_0}$. In the (U, V) chart, $U = \frac{x-x_0}{y-y_0}$ and $V = y - y_0$. Thus, the blow-up is a coordinate substitution such that

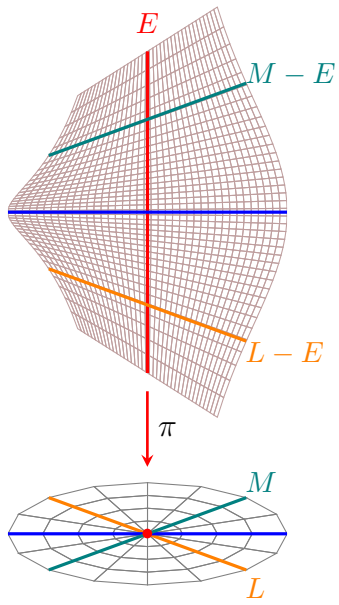

Figure 4: Visualization of the Blow-Up Procedure. Image by Anton Dzhamay, used with permission.

$x = u + x_0 = UV + x_0$ and $y = uv + y_0 = V + y_0$. In the (u, v) chart, the line $u = 0$ corresponds to the exceptional divisor, and in the (U, V) chart, the line $V = 0$ corresponds to the exceptional divisor. When we evaluate our previously indeterminate mapping in the correct blow-up chart, we get some cancellation of zeroes that resolves the indeterminacy.

After we have blown up all the necessary points (explained in a later section), we will have some rational algebraic surface, $\mathcal{X}$. This surface will have an associated lattice called the Picard lattice, denoted $\text{Pic}(\mathcal{X})$. The Picard lattice is a free abelian group generated by classes of certain basic curves. The Picard lattice of $\mathbb{P}^1 \times \mathbb{P}^1$ is generated by classes of coordinate lines (e.g. $\mathcal{H}_x$ and $\mathcal{H}_y$). Each time we blow up a point, we add an extra element to the basis of the Picard lattice, namely the class of the exceptional divisor of the blow-up. Notationally, $\mathcal{E}_i$ corresponds to the class of the exceptional divisor E_i, so $\mathcal{E}_i = [E_i]$ with respect to linear equivalence. Similarly, $\mathcal{H}_x = [H_{x=a}]$ and $\mathcal{H}_y = [H_{y=a}]$.

The Picard lattice also has the additional structure of an intersection product, denoted by $\bullet$. For example, $\mathcal{H}_x \bullet \mathcal{H}_y = 1$, since a horizontal line and vertical line will intersect once. By considering the intersection product of a class with itself, one can determine the self-intersection index of a class. For example, $\mathcal{H}_x \bullet \mathcal{H}_x = 0$, since two vertical lines will not intersect, and the same for $\mathcal{H}_y \bullet \mathcal{H}_y$. Notably, it is also possible for a self-intersection number to be negative. For classes of exceptional divisors, $\mathcal{E} \bullet \mathcal{E} = -1$, and we also encounter a self-intersection index of -2 or lower. Such curves are of special interest, as demonstrated in a later section.

4 The Applied Example

The particular example for this article comes from the study of orthogonal polynomials. This discrete Painlevé equation comes from Min and Wang in [9], who studied polynomials orthogonal to a Gaussian weight with a jump. Such polynomials satisfy the so-called three-term recurrence relation, and the coefficients in this relation evolve according to this discrete Painlevé equation. After relabeling, we get the recurrence relation

$$\begin{cases} 2x + 2\overline{x} - 2n - 1 = 2y(sy), \\ (2x - n)^2 = 4x\underline{y}y. \end{cases} \tag{1}$$

We will use the following notation: $x = x_n$, $\overline{x} = x_{n+1}$, and $\underline{x} = x_{n-1}$, and the same for y.

We can solve the above recurrence relations for $\overline{x}$ and $\underline{y}$ in terms of x and y. Furthermore, by decrementing the value of the index in the first equation, we can solve for $\underline{x}$ in terms of x and $\underline{y}$. Similarly, by incrementing the value of the index in the second equation, we can solve for $\overline{y}$ in terms of $\overline{x}$ and y. This gives the following mappings:

$$\begin{aligned}
\text{Forward step:} &\begin{cases} \overline{x} = \dfrac{1}{2} + n - x + sy - y^2, \\ \overline{y} = \dfrac{(1+n-2\overline{x})^2}{4\overline{x}y}. \end{cases} \\
\text{Backward step:} &\begin{cases} \underline{x} = -\dfrac{1}{2} + n - 2x + s\underline{y} - \underline{y}^2, \\ \underline{y} = \dfrac{(n-2x)^2}{4xy}. \end{cases}
\end{aligned} \tag{2}$$

After substituting, we get the following birational maps:

$$\begin{cases} \varphi(x,y) = \left(\dfrac{1}{2} + n - x + sy - y^2, \dfrac{(n-2(x+y(-s+y)))^2}{2y(-1-2n+2x-2sy+2y^2} \right), \\ \varphi^{-1}(x,y) = \left(-\dfrac{(n-2x)^4 - 4s(n-2x)^2xy + 8x^2(1-2n+2x)y^2}{16x^2y^2}, \dfrac{(n-2x)^2}{4xy} \right). \end{cases} \tag{3}$$

We consider φ the forward step and φ^{-1} the backward step.

5 Determining the Surface $\mathcal{X}$ and its Type

These mappings are well defined for all points in $\mathbb{P}^1 \times \mathbb{P}^1$ except where the numerator and denominator of a mapping both vanish. Such points are called indeterminacies or base points. Using a computer algebra system, we can see that the mappings are indeterminate for the points $q_1(x = \frac{n}{2}, y = 0)$, $q_3(x = 0, Y = 0)$, and $q_4(X = 0, Y = 0)$. The reasoning for this choice of indices will become apparent later.

These three base points occur in the affine charts, which are the 4 original charts on our $\mathbb{P}^1 \times \mathbb{P}^1$ space. However, we must also check for any more indeterminate points that are infinitely close to these base points. To compute such points, we can use the blow-up procedure on our known base points and determine any indeterminacies on our new exceptional divisors using the new charts.

After blowing-up, we must continue this process until no more indeterminacies are identified. Completing this process, we find the following cascades.

$$\begin{aligned} & q_1\left(x=\frac{n}{2}, y=0\right) \leftarrow q_2(u_1=0, v_1=0), \\ & q_3(x=0, Y=0), \\ & q_4(X=0, Y=0) \leftarrow q_5(U_4=0, V_4=0) \leftarrow q_6(U_5=-1, V_5=0) \\ & \quad \leftarrow q_7(U_6=-s, V_6=0) \leftarrow q_8\left(U_7=-\frac{1}{2}-n-s^2, V_7=0\right). \end{aligned} \tag{4}$$

At this point, we see that the forward and the backward maps are completely resolved. We can now construct a diagram showing the relationship between our $\mathbb{P}^1 \times \mathbb{P}^1$ space and our rational surface, $\mathcal{X}$. In this diagram (5), red lines correspond to -1 curves and blue lines correspond to -2 curves. The index of a curve is the self-intersection number of its class, which is obtained from the intersection product on $\mathrm{Pic}(\mathcal{X})$.

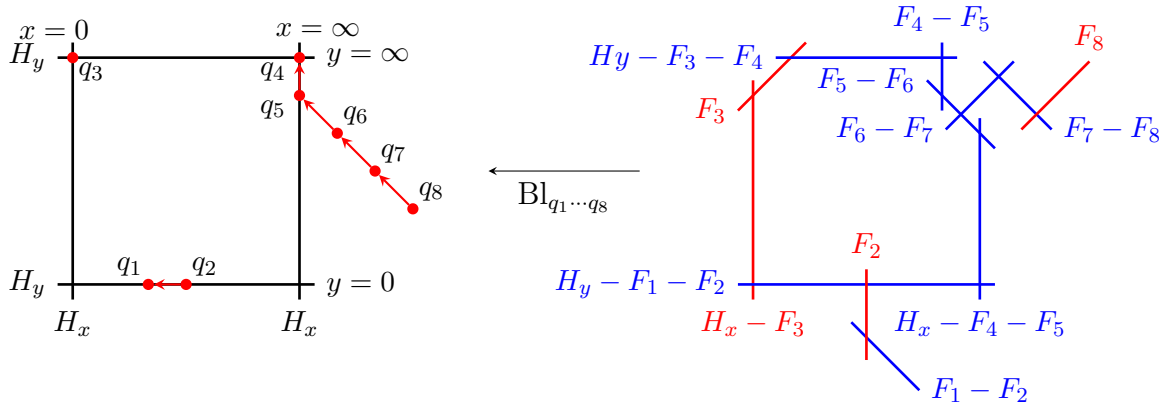

Figure 5: The Base Point Configuration and Visualization of the Surface $\mathcal{X}$.

6 Identifying the Surface Type and Induced Dynamics on the Picard Lattice

Since we have the diagram of our surface $\mathcal{X}$, we can construct the Dynkin diagram of our surface roots (6). The surface roots correspond to the irreducible components of the anti-canonical divisor class, $-K_{\mathcal{X}} = 2\mathcal{H}_x + 2\mathcal{H}_y - \mathcal{F}_{12345678}$. For brevity, we introduce the notation $-\mathcal{F}_{ij\ldots k} = -\mathcal{F}_i - \mathcal{F}_j - \ldots - \mathcal{F}_k$. Almost all -2 curves on our rational surface corresponds to a node of this Dynkin diagram, and intersecting curves correspond to connected nodes. The curve $F_1 - F_2$, however, is not a surface root, since it is disjoint from $-K_{\mathcal{X}}$. Such curves are called nodal curves, and they are outside the scope of this thesis. While the Dynkin diagram can be relabeled up to its symmetries, this particular labeling of deltas was chosen to make the upcoming change of basis clearer. By matching this diagram to the geometry of the canonical examples in [15], we see that this configuration of surface roots defines an $A_2^{(1)}/E_6^{(1)}$ surface.

$$\begin{aligned}
\delta_0 &= \mathcal{F}_7 - \mathcal{F}_8, \\
\delta_1 &= \mathcal{H}_y - \mathcal{F}_{12}, \\
\delta_2 &= \mathcal{H}_x - \mathcal{F}_{45}, \\
\delta_3 &= \mathcal{F}_5 - \mathcal{F}_6, \\
\delta_4 &= \mathcal{F}_4 - \mathcal{F}_5, \\
\delta_5 &= \mathcal{H}_y - \mathcal{F}_{34}, \\
\delta_6 &= \mathcal{F}_6 - \mathcal{F}_7.
\end{aligned}$$

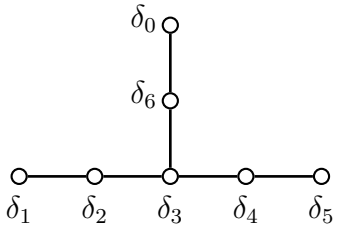

$$\begin{aligned}
\delta_0 &= \mathcal{E}_7 - \mathcal{E}_8, \\
\delta_1 &= \mathcal{E}_1 - \mathcal{E}_2, \\
\delta_2 &= \mathcal{H}_q - \mathcal{E}_{15}, \\
\delta_3 &= \mathcal{E}_5 - \mathcal{E}_6, \\
\delta_4 &= \mathcal{H}_p - \mathcal{E}_{35}, \\
\delta_5 &= \mathcal{E}_3 - \mathcal{E}_4, \\
\delta_6 &= \mathcal{E}_6 - \mathcal{E}_7.
\end{aligned}$$

Figure 6: The Surface Root Dynkin Diagram, With Roots for the Applied Example (Left) and Standard Example (Right). This diagram is known as an affine Dynkin diagram of type $E_6^{(1)}$.

At this point, we can construct a preliminary change of basis between our $\mathrm{Pic}(\mathcal{X})$ and the standard Picard lattice. This can be done by creating a system of equations by equating each δ_i of our surface to δ_i in the standard example. For future convenience, we relabeled

$\mathcal{H}_1$ from [15] as $\mathcal{H}_q$ and $\mathcal{H}_2$ as $\mathcal{H}_p$. Thus, the preliminary change of basis can be computed from the following system of equations.

$$\begin{aligned}
\mathcal{H}_y - \mathcal{F}_1 - \mathcal{F}_2 &= \mathcal{E}_1 - \mathcal{E}_2, & \mathcal{F}_5 - \mathcal{F}_6 &= \mathcal{E}_5 - \mathcal{E}_6,\\
\mathcal{H}_y - \mathcal{F}_3 - \mathcal{F}_4 &= \mathcal{E}_3 - \mathcal{E}_4, & \mathcal{F}_6 - \mathcal{F}_7 &= \mathcal{E}_6 - \mathcal{E}_7,\\
\mathcal{H}_x - \mathcal{F}_4 - \mathcal{F}_5 &= \mathcal{H}_q - \mathcal{E}_1 - \mathcal{E}_5, & \mathcal{F}_7 - \mathcal{F}_8 &= \mathcal{E}_7 - \mathcal{E}_8.\\
\mathcal{F}_4 - \mathcal{F}_5 &= \mathcal{H}_p - \mathcal{E}_3 - \mathcal{E}_5,
\end{aligned} \tag{5}$$

To compute the change of basis, we must either compute each element of our Picard lattice in terms of elements of the standard Picard lattice, or vice versa. One label mapping that satisfies the system of equations is

$$\begin{aligned}
\mathcal{H}_x &= \mathcal{H}_q + \mathcal{H}_p - \mathcal{E}_1 - \mathcal{E}_3, & \mathcal{H}_q &= \mathcal{H}_x + \mathcal{H}_y - \mathcal{F}_1 - \mathcal{F}_4,\\
\mathcal{H}_y &= \mathcal{H}_p, & \mathcal{H}_p &= \mathcal{H}_y,\\
\mathcal{F}_1 &= \mathcal{H}_p - \mathcal{E}_1, & \mathcal{E}_1 &= \mathcal{H}_y - \mathcal{F}_1,\\
\mathcal{F}_2 &= \mathcal{E}_2, & \mathcal{E}_2 &= \mathcal{F}_2,\\
\mathcal{F}_3 &= \mathcal{E}_4, & \mathcal{E}_3 &= \mathcal{H}_y - \mathcal{F}_4,\\
\mathcal{F}_4 &= \mathcal{H}_p - \mathcal{E}_3, & \mathcal{E}_4 &= \mathcal{F}_3,\\
\mathcal{F}_5 &= \mathcal{E}_5, & \mathcal{E}_5 &= \mathcal{F}_5,\\
\mathcal{F}_6 &= \mathcal{E}_6, & \mathcal{E}_6 &= \mathcal{F}_6,\\
\mathcal{F}_7 &= \mathcal{E}_7, & \mathcal{E}_7 &= \mathcal{F}_7,\\
\mathcal{F}_8 &= \mathcal{E}_8. & \mathcal{E}_8 &= \mathcal{F}_8.
\end{aligned} \tag{6}$$

Note that we could reorient our Dynkin diagram through various symmetries that would change how we match the surface roots of the two Picard lattices, hence why our first change of basis is only preliminary.

Now that we have matched geometries, we must determine the induced dynamics on $\mathrm{Pic}(\mathcal{X})$. Let φ_* be the function from $\mathrm{Pic}(\mathcal{X})$ to itself induced by the dynamics of φ. One can compute how our exceptional divisors evolve, as well as the three other -2 curves, directly from our mappings in different charts. The evolution is written below, where left arrows indicate action under φ_*^{-1} and right arrows indicate action under φ_*.

$$\begin{aligned}
\mathcal{F}_7 - \mathcal{F}_8 &\leftarrow \mathcal{H}_y - \mathcal{F}_1 - \mathcal{F}_2, & \mathcal{H}_x - \mathcal{F}_4 - \mathcal{F}_5 &\leftarrow \mathcal{F}_4 - \mathcal{F}_5,\\
\mathcal{H}_y - \mathcal{F}_1 - \mathcal{F}_2 &\leftarrow \mathcal{H}_y - \mathcal{F}_3 - \mathcal{F}_4, & \mathcal{F}_5 - \mathcal{F}_6 &\leftarrow \mathcal{F}_5 - \mathcal{F}_6,\\
\mathcal{F}_6 - \mathcal{F}_7 &\leftarrow \mathcal{H}_x - \mathcal{F}_4 - \mathcal{F}_5, & \mathcal{F}_4 - \mathcal{F}_5 &\leftarrow \mathcal{F}_6 - \mathcal{F}_7,\\
\mathcal{F}_1 - \mathcal{F}_2 &\leftarrow \mathcal{F}_1 - \mathcal{F}_2, & \mathcal{H}_y - \mathcal{F}_3 - \mathcal{F}_4 &\leftarrow \mathcal{F}_7 - \mathcal{F}_8,\\
\mathcal{H}_x + 2\mathcal{H}_y - \mathcal{F}_1 - \mathcal{F}_4 - \mathcal{F}_5 - \mathcal{F}_6 - \mathcal{F}_7 &\leftarrow \mathcal{F}_2, & \mathcal{F}_3 &\leftarrow \mathcal{F}_8.\\
\mathcal{H}_x + 2\mathcal{H}_y - \mathcal{F}_4 - \mathcal{F}_5 - \mathcal{F}_6 - \mathcal{F}_7 - \mathcal{F}_8 &\leftarrow \mathcal{F}_3,
\end{aligned} \tag{7}$$

$$\begin{aligned}
\mathcal{H}_y - \mathcal{F}_1 - \mathcal{F}_2 &\rightarrow \mathcal{H}_y - \mathcal{F}_3 - \mathcal{F}_4, & \mathcal{F}_4 - \mathcal{F}_5 &\rightarrow \mathcal{F}_6 - \mathcal{F}_7,\\
\mathcal{H}_y - \mathcal{F}_3 - \mathcal{F}_4 &\rightarrow \mathcal{F}_7 - \mathcal{F}_8, & \mathcal{F}_5 - \mathcal{F}_6 &\rightarrow \mathcal{F}_5 - \mathcal{F}_6,\\
\mathcal{H}_x - \mathcal{F}_4 - \mathcal{F}_5 &\rightarrow \mathcal{F}_4 - \mathcal{F}_5, & \mathcal{F}_6 - \mathcal{F}_7 &\rightarrow \mathcal{H}_x - \mathcal{F}_4 - \mathcal{F}_5,\\
\mathcal{F}_1 - \mathcal{F}_2 &\rightarrow \mathcal{F}_1 - \mathcal{F}_2, & \mathcal{F}_7 - \mathcal{F}_8 &\rightarrow \mathcal{H}_y - \mathcal{F}_1 - \mathcal{F}_2,\\
\mathcal{F}_2 &\rightarrow \mathcal{H}_x - \mathcal{F}_1, & \mathcal{F}_8 &\rightarrow \mathcal{H}_x - \mathcal{F}_3.\\
\mathcal{F}_3 &\rightarrow \mathcal{F}_8,
\end{aligned} \tag{8}$$

Treating the above evolution as two linear systems of equations of 10 variables, namely $\mathcal{H}_x, \mathcal{H}_y$, and $\mathcal{F}_{1\cdots 8}$, we can directly compute the mappings of these individual classes under

φ_* and φ_*^{-1}. The mapping under φ_* is as follows:

$$\begin{aligned}
&\mathcal{H}_x \to 4\mathcal{H}_x + 2\mathcal{H}_y - \mathcal{F}_{1122334567}, && \mathcal{F}_4 \to 2\mathcal{H}_x + \mathcal{H}_y - \mathcal{F}_{12347},\\
&\mathcal{H}_y \to 2\mathcal{H}_x + \mathcal{H}_y - \mathcal{F}_{1234}, && \mathcal{F}_5 \to 2\mathcal{H}_x + \mathcal{H}_y - \mathcal{F}_{12346},\\
&\mathcal{F}_1 \to \mathcal{H}_x - \mathcal{F}_2, && \mathcal{F}_6 \to 2\mathcal{H}_x + \mathcal{H}_y - \mathcal{F}_{12345},\\
&\mathcal{F}_2 \to \mathcal{H}_x - \mathcal{F}_1, && \mathcal{F}_7 \to \mathcal{H}_x + \mathcal{H}_y - \mathcal{F}_{123},\\
&\mathcal{F}_3 \to \mathcal{F}_8, && \mathcal{F}_8 \to \mathcal{H}_x - \mathcal{F}_3.
\end{aligned} \tag{9}$$

The mapping under φ_*^{-1} is as follows:

$$\begin{aligned}
&\mathcal{H}_x \to \mathcal{H}_x + 2\mathcal{H}_y - \mathcal{F}_{4567}, && \mathcal{F}_4 \to \mathcal{H}_x + \mathcal{H}_y - \mathcal{F}_{456},\\
&\mathcal{H}_y \to 2\mathcal{H}_x + 4\mathcal{H}_y - \mathcal{F}_{1244556678}, && \mathcal{F}_5 \to \mathcal{H}_y - \mathcal{F}_6,\\
&\mathcal{F}_1 \to \mathcal{H}_x + 2\mathcal{H}_y - \mathcal{F}_{24567}, && \mathcal{F}_6 \to \mathcal{H}_y - \mathcal{F}_5,\\
&\mathcal{F}_2 \to \mathcal{H}_x + 2\mathcal{H}_y - \mathcal{F}_{14567}, && \mathcal{F}_7 \to \mathcal{H}_y - \mathcal{F}_4,\\
&\mathcal{F}_3 \to \mathcal{H}_x + 2\mathcal{H}_y - \mathcal{F}_{45678}, && \mathcal{F}_8 \to \mathcal{F}_3.
\end{aligned} \tag{10}$$

7 Comparing the Dynamics and Determining the Final Change of Basis

We can now compare the dynamics of our applied example to the dynamics of the standard example. To compare the dynamics on the level of translation elements, we need to determine the symmetry roots of our surface. The symmetry roots are classes in the Picard lattice that are orthogonal to each of the surface roots. These are notable since reflections about these symmetry roots fix the geometry of our surface. We can determine the symmetry roots of our example by applying the label mapping to the symmetry roots of the standard example.

$$
\begin{aligned}
\alpha_0 &= \mathcal{H}_q + \mathcal{H}_p - \mathcal{E}_5 - \mathcal{E}_6 - \mathcal{E}_7 - \mathcal{E}_8 \\
&= (\mathcal{H}_x + \mathcal{H}_y - \mathcal{F}_1 - \mathcal{F}_4) + (\mathcal{H}_y) - (\mathcal{F}_5) - (\mathcal{F}_6) - (\mathcal{F}_7) - (\mathcal{F}_8) \\
&= \mathcal{H}_x + 2\mathcal{H}_y - \mathcal{F}_1 - \mathcal{F}_4 - \mathcal{F}_5 - \mathcal{F}_6 - \mathcal{F}_7 - \mathcal{F}_8 \\
\alpha_1 &= \mathcal{H}_q - \mathcal{E}_3 - \mathcal{E}_4 = (\mathcal{H}_x + \mathcal{H}_y - \mathcal{F}_1 - \mathcal{F}_4) - (\mathcal{H}_y - \mathcal{F}_4) - (\mathcal{F}_3) \\
&= \mathcal{H}_x - \mathcal{F}_1 - \mathcal{F}_3 \\
\alpha_2 &= \mathcal{H}_p - \mathcal{E}_1 - \mathcal{E}_2 = (\mathcal{H}_y) - (\mathcal{H}_y - \mathcal{F}_1) - (\mathcal{F}_2) \\
&= \mathcal{F}_1 - \mathcal{F}_2
\end{aligned}
\tag{11}
$$

These α roots are the symmetry roots of our example.

$$
\begin{aligned}
\alpha_0 &= \mathcal{H}_x + 2\mathcal{H}_y - \mathcal{F}_{145678} \\
\alpha_1 &= \mathcal{H}_x - \mathcal{F}_{13} \\
\alpha_2 &= \mathcal{F}_1 - \mathcal{F}_2
\end{aligned}
$$

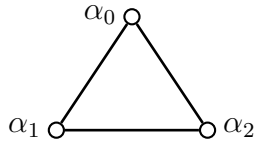

$$
\begin{aligned}
\alpha_0 &= \mathcal{H}_q + \mathcal{H}_p - \mathcal{E}_{5678} \\
\alpha_1 &= \mathcal{H}_q - \mathcal{E}_{34} \\
\alpha_2 &= \mathcal{H}_p - \mathcal{E}_{12}
\end{aligned}
$$

Figure 7: The Symmetry Root Dynkin Diagram, With Roots for the Applied Example (Left) and Standard Example (Right). This diagram is known as an affine Dynkin diagram of type $A_2^{(1)}$.

Let δ be the anti-canonical divisor class $-K_{\mathcal{X}} = 2\mathcal{H}_x + 2\mathcal{H}_y - \mathcal{F}_{12345678}$. We can now use the divisor mapping we computed earlier to determine the evolution of our α roots. For example, the mapping of α_0 under φ_* can be computed as follows:

$$
\begin{aligned}
\alpha_0 &= \mathcal{H}_x + 2\mathcal{H}_y - \mathcal{F}_1 - \mathcal{F}_4 - \mathcal{F}_5 - \mathcal{F}_6 - \mathcal{F}_7 - \mathcal{F}_8 \\
&\longmapsto (4\mathcal{H}_x + 2\mathcal{H}_y - 2\mathcal{F}_{1122334567}) + 2(2\mathcal{H}_x + \mathcal{H}_y - \mathcal{F}_{1234}) - (\mathcal{H}_x - \mathcal{F}_2) \\
&\qquad - (2\mathcal{H}_x + \mathcal{H}_y - \mathcal{F}_{12347}) - (2\mathcal{H}_x + \mathcal{H}_y - \mathcal{F}_{12346}) - (2\mathcal{H}_x + \mathcal{H}_y - \mathcal{F}_{12345}) \\
&\qquad - (\mathcal{H}_x + \mathcal{H}_y - \mathcal{F}_{123}) - (\mathcal{H}_x - \mathcal{F}_3) \\
&= (\mathcal{H}_x + 2\mathcal{H}_y - \mathcal{F}_{145678}) - (2\mathcal{H}_x + 2\mathcal{H}_y - \mathcal{F}_{12345678}) \\
&= \alpha_0 - \delta
\end{aligned}
\tag{12}
$$

Thus, $\alpha_0 \mapsto \alpha_0 - \delta$. Using similar computations, we find that $\alpha_1 \mapsto \alpha_1 + \delta$ and $\alpha_2 \mapsto \alpha_2$. Let $\vec{\alpha} = \langle \alpha_0, \alpha_1, \alpha_2 \rangle$. We expect the dynamics of the α roots to be a translation by a vector times δ. Indeed, we find the following dynamics of $\vec{\alpha}$ under φ_*:

$$\varphi_*(\vec{\alpha}) = \vec{\alpha} + \langle -1, 1, 0 \rangle \delta \tag{13}$$

Let ψ_* be the dynamics of the standard example from [15]. We know $\psi_*(\vec{\alpha}) = \vec{\alpha} + \langle 0, 1, -1 \rangle \delta$. This is a different translation vector from our applied dynamic, which we will show to be conjugated. Thus, we need to adjust our change of basis so our translation vector matches the standard translation vector.

To adjust our change of basis, we must express φ_* and ψ_* in terms of generators of the extended affine Weyl group of our surface, $\widetilde{W}\left(A_2^{(1)}\right)$. The extended affine Weyl group is a group of symmetries generating the dynamics defined as the semidirect product $\mathrm{Aut}\left(A_2^{(1)}\right) \ltimes W\left(A_2^{(1)}\right)$. $\mathrm{Aut}\left(A_2^{(1)}\right)$ is the same as the group of automorphisms of the symmetry root diagram, which is isomorphic to the dihedral group D_3. Thus, it can be generated by the reflections defined in the diagram below. $W\left(A_2^{(1)}\right)$ can be generated by $w_i = r_{\alpha_i}$, which acts on $\mathrm{Pic}(\mathcal{X})$ as defined below. The group $\widetilde{W}\left(A_2^{(1)}\right)$ is generated by the union of these generators.

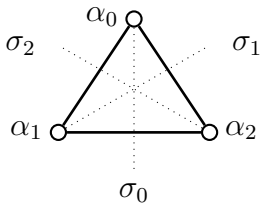

$$w_i(C) = r_{\alpha_i}(C) = C + (C \bullet \alpha_i)\alpha_i,$$
where $C \in \mathrm{Pic}(\mathcal{X})$

Figure 8: Generators of $\widetilde{W}\left(A_2^{(1)}\right)$

To decompose our translation vectors, we can apply the generators of $\widetilde{W}$ to $\vec{\alpha}$ such that it acts of the components of the vector α_i the same way it would act on the surface roots α_i.

Note that $\delta = \alpha_0 + \alpha_1 + \alpha_2$. Thus, we can decompose ψ_* in following way. We want to find the series of elements that can invert the mapping such that $\psi_* \circ \cdots$ is the identity element. Thus, we want to act by elements until our translation vector becomes the zero vector. We introduce the notation $\alpha_{ij\ldots k} = \alpha_i + \alpha_j + \ldots + \alpha_k$.

$$\begin{aligned}
\psi_* &= \langle \alpha_0, \alpha_1 + \delta, \alpha_2 - \delta \rangle \\
&= \langle \alpha_0, \alpha_{0112}, -\alpha_{01} \rangle \\
\psi_* \circ w_2 &= \langle \alpha_0 + (-\alpha_{01}), \alpha_{0112} + (-\alpha_{01}), -(-\alpha_{01}) \rangle \\
&= \langle -\alpha_1, \alpha_{12}, \alpha_{01} \rangle \\
\psi_* \circ w_2 \circ w_0 &= \langle \alpha_1, \alpha_2, \alpha_0 \rangle \\
\psi_* \circ w_2 \circ w_0 \circ \sigma_1 &= \langle \alpha_0, \alpha_2, \alpha_1 \rangle \\
\psi_* \circ w_2 \circ w_0 \circ \sigma_1 \circ \sigma_0 &= \langle \alpha_0, \alpha_1, \alpha_2 \rangle
\end{aligned} \tag{14}$$

Thus, $\psi_* \circ w_2 \circ w_0 \circ \sigma_1 \circ \sigma_0 = \mathrm{id}$, the identity element of $\widetilde{W}$. Each of those generators are involutions, so that equation can be rewritten as $\psi_* = \sigma_0 \circ \sigma_1 \circ w_0 \circ w_2$. This is the decomposition of ψ_* into generators of $\widetilde{W}$. Similarly, we can decompose φ_* into generators using the same process.

$$\begin{aligned}
\varphi_* &= \langle \alpha_0 - \delta, \alpha_1 + \delta, \alpha_2 \rangle \\
&= \langle -\alpha_{12}, \alpha_{0112}, \alpha_2 \rangle \\
\varphi_* \circ w_0 &= \langle \alpha_{12}, \alpha_{01}, -\alpha_1 \rangle \\
\varphi_* \circ w_0 \circ w_2 &= \langle \alpha_2, \alpha_0, \alpha_1 \rangle \\
\varphi_* \circ w_0 \circ w_2 \circ \sigma_2 &= \langle \alpha_0, \alpha_2, \alpha_1 \rangle \\
\varphi_* \circ w_0 \circ w_2 \circ \sigma_2 \circ \sigma_0 &= \langle \alpha_0, \alpha_1, \alpha_2 \rangle
\end{aligned} \tag{15}$$

Thus $\varphi_* \circ w_0 \circ w_2 \circ \sigma_2 \circ \sigma_0 = \mathrm{id}$, so $\varphi_* = \sigma_0 \circ \sigma_2 \circ w_2 \circ w_0$. We have now decomposed both

mappings into generators of $\widetilde{W}$. The next step is to describe φ_* as a conjugation of ψ_*. Note that the translation vectors for ψ_* are φ_* are nearly the same, but with their first and third entries swapped. This suggests that σ_1, which simply swaps the first and second entries of $\vec{\alpha}$, will be the conjugation element. We can demonstrate this conjugation through swapping the positions of pairs of elements, denoted by bolded symbols in the following equations. Note that when σ_1 is "passed through" another generator, it acts on the index of that generator, i, the same way it acts on the index of α_i.

$$\begin{aligned}
\sigma_1 \circ \varphi_* \circ (\sigma_1)^{-1} &= \sigma_1 \circ \sigma_0 \circ \sigma_2 \circ w_2 \circ w_0 \circ \sigma_1 \\
&= \sigma_1 \circ \sigma_0 \circ \sigma_2 \circ w_2 \circ \boldsymbol{\sigma_1} \circ \boldsymbol{w_2} \\
&= \sigma_1 \circ \sigma_0 \circ \sigma_2 \circ \boldsymbol{\sigma_1} \circ \boldsymbol{w_0} \circ w_2 \\
&= \sigma_1 \circ \boldsymbol{\sigma_1} \circ \boldsymbol{\sigma_0} \circ \sigma_1 \circ w_0 \circ w_2 \\
&= (\sigma_1 \circ \sigma_1) \circ \sigma_0 \circ \sigma_1 \circ w_0 \circ w_2 \\
&= \sigma_0 \circ \sigma_1 \circ w_0 \circ w_2 \\
&= \psi_*
\end{aligned} \tag{16}$$

This demonstrates that we can indeed write ψ_* as $\sigma_1 \circ \varphi_* \circ (\sigma_1)^{-1}$.

Now that we have a conjugation between ψ_* and φ_*, we can use this conjugation element to adjust our preliminary change of basis to the final change of basis. Note that σ_1 acts on the Picard lattice as a sequence of three reflections: reflecting over $\mathcal{H}_q - \mathcal{E}_5 - \mathcal{E}_6$, reflecting over $\mathcal{E}_1 - \mathcal{E}_7$, and reflecting over $\mathcal{E}_2 - \mathcal{E}_8$. First, it is convenient to apply σ_1 to our basis of the Picard lattice of the standard example.

$$
\begin{aligned}
\sigma_1(\mathcal{H}_q) &= \mathcal{H}_q, & \sigma_1(\mathcal{E}_4) &= \mathcal{E}_4, \\
\sigma_1(\mathcal{H}_p) &= \mathcal{H}_q + \mathcal{H}_p - \mathcal{E}_5 - \mathcal{E}_6, & \sigma_1(\mathcal{E}_5) &= \mathcal{H}_q - \mathcal{E}_6, \\
\sigma_1(\mathcal{E}_1) &= \mathcal{E}_7, & \sigma_1(\mathcal{E}_6) &= \mathcal{H}_q - \mathcal{E}_5, \\
\sigma_1(\mathcal{E}_2) &= \mathcal{E}_8, & \sigma_1(\mathcal{E}_7) &= \mathcal{E}_1, \\
\sigma_1(\mathcal{E}_3) &= \mathcal{E}_3, & \sigma_1(\mathcal{E}_8) &= \mathcal{E}_2.
\end{aligned} \tag{17}
$$

With the mapping of these individual classes under σ_1, we can compute the final change of basis through substitution. The label mapping for $\mathcal{H}_x$ is computed as an example.

$$
\begin{aligned}
\mathcal{H}_x &= \sigma_1(\mathcal{H}_q + \mathcal{H}_p - \mathcal{E}_1 - \mathcal{E}_3) \\
&= \sigma_1(\mathcal{H}_q) + \sigma_1(\mathcal{H}_p) - \sigma_1(\mathcal{E}_1) - \sigma_1(\mathcal{E}_3) \\
&= (\mathcal{H}_q) + (\mathcal{H}_q + \mathcal{H}_p - \mathcal{E}_5 - \mathcal{E}_6) - (\mathcal{E}_7) - (\mathcal{E}_3) \\
&= 2\mathcal{H}_q + \mathcal{H}_p - \mathcal{E}_3 - \mathcal{E}_5 - \mathcal{E}_6 - \mathcal{E}_7
\end{aligned} \tag{18}
$$

Using the same process for each element of the basis for the standard Picard lattice, and then solving for the inverse change of basis as well, we get the following relationships.

$$
\begin{aligned}
\mathcal{H}_x &= 2\mathcal{H}_q + \mathcal{H}_p - \mathcal{E}_3 - \mathcal{E}_5 - \mathcal{E}_6 - \mathcal{E}_7, & \mathcal{H}_q &= \mathcal{H}_x + \mathcal{H}_y - \mathcal{F}_1 - \mathcal{F}_4,\\
\mathcal{H}_y &= \mathcal{H}_q + \mathcal{H}_p - \mathcal{E}_5 - \mathcal{E}_6, & \mathcal{H}_p &= \mathcal{H}_x + 2\mathcal{H}_y - \mathcal{F}_1 - \mathcal{F}_4 - \mathcal{F}_5 - \mathcal{F}_6,\\
\mathcal{F}_1 &= \mathcal{H}_q + \mathcal{H}_p - \mathcal{E}_5 - \mathcal{E}_6 - \mathcal{E}_7, & \mathcal{E}_1 &= \mathcal{F}_7,\\
\mathcal{F}_2 &= \mathcal{E}_8, & \mathcal{E}_2 &= \mathcal{F}_8,\\
\mathcal{F}_3 &= \mathcal{E}_4, & \mathcal{E}_3 &= \mathcal{H}_y - \mathcal{F}_4,\\
\mathcal{F}_4 &= \mathcal{H}_q + \mathcal{H}_p - \mathcal{E}_3 - \mathcal{E}_5 - \mathcal{E}_6, & \mathcal{E}_4 &= \mathcal{F}_3,\\
\mathcal{F}_5 &= \mathcal{H}_q - \mathcal{E}_6, & \mathcal{E}_5 &= \mathcal{H}_x + \mathcal{H}_y - \mathcal{F}_1 - \mathcal{F}_4 - \mathcal{F}_6,\\
\mathcal{F}_6 &= \mathcal{H}_p - \mathcal{E}_5, & \mathcal{E}_6 &= \mathcal{H}_x + \mathcal{H}_y - \mathcal{F}_1 - \mathcal{F}_4 - \mathcal{F}_5,\\
\mathcal{F}_7 &= \mathcal{E}_1, & \mathcal{E}_7 &= \mathcal{H}_y - \mathcal{F}_1,\\
\mathcal{F}_8 &= \mathcal{E}_2. & \mathcal{E}_8 &= \mathcal{F}_2.
\end{aligned}
\tag{19}
$$

This new change of basis results in the following labeling of surface roots:

$$
\begin{aligned}
\delta_0 &= \mathcal{H}_y - \mathcal{F}_1 - \mathcal{F}_2, & \delta_4 &= \mathcal{F}_5 - \mathcal{F}_5,\\
\delta_1 &= \mathcal{F}_7 - \mathcal{F}_8, & \delta_5 &= \mathcal{H}_y - \mathcal{F}_3 - \mathcal{F}_4,\\
\delta_2 &= \mathcal{F}_6 - \mathcal{F}_7, & \delta_6 &= \mathcal{H}_x - \mathcal{F}_4 - \mathcal{F}_5.\\
\delta_3 &= \mathcal{F}_5 - \mathcal{F}_6,
\end{aligned}
\tag{20}
$$

and the following labeling of symmetry roots:

$$
\begin{aligned}
\alpha_0 &= \mathcal{F}_1 - \mathcal{F}_2,\\
\alpha_1 &= \mathcal{H}_x - \mathcal{F}_1 - \mathcal{F}_3,\\
\alpha_2 &= \mathcal{H}_x + 2\mathcal{H}_y - \mathcal{F}_1 - \mathcal{F}_4 - \mathcal{F}_5 - \mathcal{F}_6 - \mathcal{F}_7 - \mathcal{F}_8.
\end{aligned}
\tag{21}
$$

Using the same procedure from the beginning of this section with these new symmetry

roots, we compute that $\varphi_*(\vec{\alpha}) = \psi_*(\vec{\alpha}) = \vec{\alpha} + \langle 0, 1, -1 \rangle \delta$. This confirms that this final change of basis is the label mapping that matches the two dynamics.

8 Determining the Change of Coordinates

Now that we have the correct change of basis from the standard example to our applied example, we need to find the explicit change of coordinates that induces that change of basis. From [15], the standard example has the following point configuration,

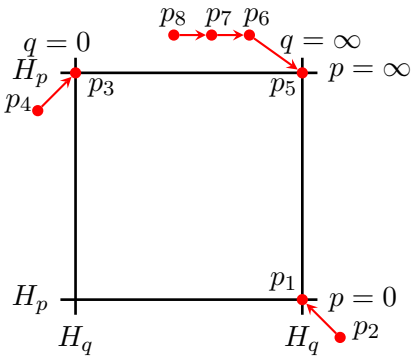

$$
\begin{aligned}
&p_1(Q = 0, p = 0) \leftarrow p_2(u_1 = 0, v_1 = -a_2),\\
&p_3(q = 0, P = 0) \leftarrow p_4(U_3 = a_1, V_3 = 0),\\
&p_5(Q = 0, P = 0) \leftarrow p_6(u_5 = 0, v_5 = 1)\\
&\qquad \leftarrow p_7(u_6 = 0, v_6 = -t) \leftarrow p_8(u_7 = 0, v_7 = a_0 + t^2).
\end{aligned}
$$

Figure 9: The Point Configuration for the Standard $A_2^{(1)}/E_6^{(1)}$ Example

the following recurrence relations,

$$
\begin{cases}
\overline{q} + q = p - t - \dfrac{a_2}{p}, \\
p + \underline{p} = q + t + \dfrac{a_1}{t}.
\end{cases}
\tag{22}
$$

and the following maps:

$$
\begin{cases}
\psi(q,p) = \left(-\dfrac{a_2}{p} + p - q - t, -\dfrac{a_2^2 + a_2 p(-p + 2q + t) + p^2(-1 + a_1 - pq + q^2 + qt)}{p(a_2 + p(-p + q + t))} \right), \\
\psi^{-1}(q,p) = \left(\dfrac{a_1^2 + a_1 q(-2p + q + t) - q^2(-1 + a_2 - p^2 + p(q + t))}{q(a_1 + q(-p + q + t))}, -p + \dfrac{a_1}{q} + q + t \right).
\end{cases}
\tag{23}
$$

Note that the information for the standard example contain a_0, a_1, and a_2. These are the root variables of this surface type, which are certain "intrinsic" parameters corresponding to symmetry roots. An explanation for how these root variables are obtained is outside the scope of this text, but the root variables for our original example are

$$a_0 = 0, \quad a_1 = -n, \quad \text{and } a_2 = n + 1. \tag{24}$$

We found from the final change of basis that $\mathcal{H}_x = 2\mathcal{H}_q + \mathcal{H}_p - \mathcal{E}_3 - \mathcal{E}_5 - \mathcal{E}_6 - \mathcal{E}_7$. This means that every vertical line in the applied example corresponds to some $(2, 1)$ curve in the standard example that passes through the points p_3, p_5, p_6, and p_7. We must find which $(2, 1)$ curves pass through those points.

Consider an arbitrary $(2, 1)$ curve, $Aq^2p + Bqp + Cp + Dq^2 + Eq + F = 0$. To force it to pass through the point p_3, we must look at this curve in the (q, P) chart: $Aq^2 + Bq + C + Dq^2P + EqP + FP = 0$. We want this equation to be true when $q = 0$ and $P = 0$.

$$\begin{aligned} Aq^2 + Bq + C + Dq^2P + EqP + FP &= 0 \\ A(0)^2 + B(0) + C + D(0)^2(0) + E(0)(0) + F(0) &= 0 \\ C &= 0 \end{aligned} \tag{25}$$

Therefore, if this curve passes through the point p_3, C must equal 0. Using similar reasoning with p_5, we find that $A = 0$. The computations for passing through points on exceptional divisors are more subtle. To force the curve to pass through the point p_6, we

must look at this curve in the (u_5, v_5) chart.

$$\begin{aligned} Bq + Dq^2P + EqP + FP &= 0 \\ BQ + DP + EQP + FQ^2P &= 0 \\ B(u_5) + D(u_5v_5) + E(u_5)(u_5v_5) + F(u_5)^2(u_5v_5) &= 0 \\ u_5(B + Dv_5 + Eu_5v_5 + Fu_5^2v_5) &= 0 \end{aligned} \tag{26}$$

Remember that we are are trying to describe the class $2\mathcal{H}_q + \mathcal{H}_p - \mathcal{E}_3 - \mathcal{E}_5 - \mathcal{E}_6 - \mathcal{E}_7$. Curves in this class are proper transforms excluding the exceptional divisors E_3, E_5, E_6, and E_7. The zero set for the equation above is the union of $\{u_5 = 0\}$, which corresponds to the class $\mathcal{E}_5$, and $\{B + Dv_5 + Eu_5v_5 + Fu_5^2v_5 = 0\}$, which corresponds to the class we want. Thus, we only consider the second factor. We want this equation to be true when $u_5 = 0$ and $v_5 = 1$.

$$\begin{aligned} B + Dv_5 + Eu_5v_5 + Fu_5^2v_5 &= 0 \\ B + D(1) + E(0)(1) + F(0)^2(1) &= 0 \\ B + D &= 0 \\ B &= -D \end{aligned} \tag{27}$$

Therefore, if the curve passes through the point p_6, B must equal $-D$. Finally, using similar reasoning with p_7, we find that $E = Dt$. Applying the information about these coefficients to the curve in the (q, p) chart, we get the curve $F + D(q^2 - qp + qt) = 0$. Thus, every vertical line in the applied example corresponds to some curve defined by a linear combination of 1 and $q^2 - qp + qt$ in the standard example. These two expressions are called the basis curves of $x(q, p)$. Using similar computations for horizontal lines, we find that the basis curves of $y(q, p)$ are 1 and $p - q$. Note that due to the automorphisms of $\mathbb{P}^1$, we could have chosen a different basis for this pencil of curves. Thus, when describing the change of

coordinates, we must consider Möbius transformations of the basis curves.

$$\begin{cases} x(q,p) = \dfrac{A + B(q^2 - qp + qt)}{C + D(q^2 - qp + qt)}, \\ y(q,p) = \dfrac{K + L(p-q)}{M + N(p-q)}. \end{cases} \tag{28}$$

To find the explicit change of coordinates between the standard example and the applied example, we must determine the values of the coefficients $A, \cdots, N$. We can determine these values by matching -1 and -2 curves on the two surfaces. Starting with -2 curves, consider the curve $H_p - E_3 - E_5$. Using the change of basis, we can see $\mathcal{H}_q - \mathcal{E}_3 - \mathcal{E}_5 = (\mathcal{H}_x + 2\mathcal{H}_y - \mathcal{F}_1 - \mathcal{F}_4 - \mathcal{F}_5 - \mathcal{F}_6) - (\mathcal{H}_y - \mathcal{F}_4) - (\mathcal{H}_x + \mathcal{H}_y - \mathcal{F}_1 - \mathcal{F}_4 - \mathcal{F}_6) = \mathcal{F}_4 - \mathcal{F}_5$. Thus, the curve $H_q - E_3 - E_5$ on the standard surface corresponds to the curve $F_4 - F_5$ on the applied surface. This means when $P = 0$, we want $X = 0$ and $Y = 0$.

$$\begin{aligned} (X(q,p), Y(q,p)) &= \left(\frac{1}{x(q,p)}, \frac{1}{y(q,p)} \right) \\ &= \left(\frac{C + D(q^2 - qp + qt)}{A + B(q^2 - qp + qt)}, \frac{M + N(p-q)}{K + L(p-q)} \right) \\ &= \left(\frac{CP + D(q^2P - q + qPt)}{AP + B(q^2P - q + qPt)}, \frac{MP + N(1 - qP)}{KP + L(1 - qP)} \right) \\ &= \left(\frac{-Dq}{-Bq}, \frac{N}{L} \right) \\ &= \left(\frac{D}{B}, \frac{N}{L} \right) \end{aligned} \tag{29}$$

In order for $\frac{D}{B}$ and $\frac{N}{L}$ to be 0, D and N must both equal 0. Furthermore, when we substitute $D = 0$ and $N = 0$ into $x(q,p)$ and $y(q,p)$, we have only constants in the denominator. Thus, the denominators can be "absorbed" into the constants in the numerator, so we have

the following expressions for x and y.

$$\begin{cases} x(q,p) = A + B(q^2 - qp + qt), \\ y(q,p) = K + L(p - q). \end{cases} \tag{30}$$

We can use similar reasoning with $H_q - E_1 - E_5$ to see that $B = -L^2$ and with $E_1 - E_2$ to see that $K = \frac{s-Lt}{2}$. The other -2 curves do not give us any new information. Thus, after matching -2 curves, we get the following expressions for x and y.

$$\begin{cases} x(q,p) = A - L^2(q^2 - qp + qt), \\ y(q,p) = \dfrac{s + L(2p - 2q - t)}{2}. \end{cases} \tag{31}$$

To identify the final constants, we must match -1 curves. The natural choices for these computations are the exceptional divisors. For example, consider the fact that E_4 corresponds with F_3. Thus, when $U_3 = a_1$ and $V_3 = 0$ on the standard surface, we want $x = 0$ and $Y = 0$ on the applied surface. These computations follow the same logic as the previous computations and are thus omitted. We find that $A = -a_1 L^2$. Similarly using the fact that E_8 corresponds to F_2, we find that $L = -\frac{s}{t}$. At this point, we have determined the values of each of the coefficients $A, \cdots, N$.

$$\begin{cases} x(q,p) = -\dfrac{s^2(q^2 - qp + qt + a_1)}{t^2}, \\ y(q,p) = \dfrac{s(q - p + t)}{t}. \end{cases} \tag{32}$$

Note that the parameter s was not defined for the standard surface. Thus, we must determine s in terms of t. Using the final divisor mapping, the fact that E_2 corresponds to F_8, we get that $s = \frac{t}{\sqrt{2}}$. Note we must also include the correspondence between root variables and n to change between the parameters of the standard example and the parameters of our example. This gives us our final change of coordinates that transforms our original example

into the standard one. Additionally, we can use this first change of coordinates to compute an inverse change of coordinates, that transforms the standard example into our original example. The two changes of coordinates are given below.

$$\begin{cases} x(q,p) = \dfrac{q(p-q-t)-a_1}{2} \\ y(q,p) = \dfrac{q+t-p}{\sqrt{2}}. \\ n = -a_1 \\ s = \dfrac{t}{\sqrt{2}} \end{cases} \tag{33}$$

$$\begin{cases} q(x,y) = \dfrac{-2x+n}{\sqrt{2}y} \\ p(x,y) = \dfrac{-2y^2-2x+2sy+n}{\sqrt{2}y} \\ t = \sqrt{2}s \\ a_0 = 0 \\ a_1 = -n \\ a_2 = n+1 \end{cases} \tag{34}$$

With these changes of coordinates, we can move between our original example and the standard $A_2^{(1)}/E_6^{(1)}$ example, demonstrating that we have identified our original equation correctly.

9 Conclusion

In this paper, we determined the surface type of an applied discrete Painlevé equation and identified an explicit change of coordinates between it and a standard example. We also demonstrated the procedure for identifying this change of coordinates in detail to serve as a model for mathematicians unfamiliar with the theory of Painlevé equations.

References

[1] Anton Dzhamay, Galina Filipuk, Adam Ligęza, and Alexander Stokes, *Hamiltonian structure for a differential system from a modified Laguerre weight via the geometry of the modified third Painlevé equation*, App. Math. Letters **120** (2021), 107248, DOI 10.1016/j.aml.2021.107248.

[2] Anton Dzhamay, Galina Filipuk, and Alexander Stokes, *Differential equations for the recurrence coefficients of semiclassical orthogonal polynomials and their relation to the Painlevé equations via the geometric approach*, Stud. Appl. Math. **148** (2022), 1656–1702, DOI 10.1111/sapm.12487.

[3] Anton Dzhamay and Tomoyuki Takenawa, *On some applications of Sakai's geometric theory of discrete Painlevé equations*, Symm., Int., and Geo.: Meth. and App. **14** (2018), 075-094, DOI 10.3842/SIGMA.2018.075.

[4] A. Dzhamay, G. Filipuk, and A. Stokes, *Recurrence coefficients for discrete orthogonal polynomials with hypergeometric weight and discrete Painlevé equations*, arXiv:1910.10981v1 [nlin.SI] 2019, 1-24.

[5] A. Dzhamay, H. Sakai, and T. Takenawa, *Discrete Schlesinger transformations, their Hamiltonian formulation, and difference Painlevé equations*, arXiv:1302.2972 [math-ph], 2014, 1-29.

[6] A. R. Its, A. V. Kitaev, A. S. Fokas, *Matrix models of two-dimensional quantum gravity and isomonodromy solutions of "discrete Painleve equations"*, Zap. Nauchn. Sem. LOMI **187** (1991), 3–30, DOI 10.1007/BF02364564.

[7] A. S. Carstea and T. Takenawa, *A note on minimization of rational surfaces obtained from birational dynamical systems*, Jour. of Nonlin. Math. Phys. **20** (2013), 17-33, DOI 10.1080/14029251.2013.862432.

[8] B. Grammaticos and A. Ramani, *Discrete Painlevé equations: a review*, Discrete integrable systems, Lecture Notes in Phys., vol. 644, Springer, Berlin, 2004, 245–321.

[9] Chau Min and Liwei Wang, *Asymptotics of the Smallest Eigenvalue Distributions of Freud Unitary Ensembles*, arXiv:2402.15190 [math-ph], 2024, 1-35.

[10] E. Brézin and V. A. Kazakov, *Exactly solvable field theories of closed strings*, Phys. Lett. B, **236** (1990), 144-150, DOI 10.1016/0370-2693(90)90818-Q.

[11] E. Laguerre, *Sur la réduction en fractions continues d'une fraction qui satisfait à une équation différentielle linéaire du premier ordre dont les coefficients sont rationnels*, Journ. de Mathé. Pures et App., **1** (1885), 135-165.

[12] H. Sakai, *Rational surfaces associated with affine root systems and geometry of the Painlevé equations*, Commun. Math. Phys. **220** (2001), 165–229, DOI 10.1007/s002200100446.

[13] Jie Hu, Anton Dzhamay, and Yang Chen, *Gap probabilities in the Laguerre unitary ensemble and discrete Painlevé equations*, J. Phys. A: Math. Theor. **53** (2020), 354003, DOI 10.1088/1751-8121/ab9f70.

[14] Jie Hu, Galina Filipuk, and Yang Chen, *Differential and difference equations for recurrence coefficients of orthogonal polynomials with hypergeometric weights and Bäcklund transformations of the sixth Painlevé equation*, Rand. Matrices: Theory and App. **10** (2021), 2150029, DOI 10.1142/S2010326321500295.

[15] Kenji Kajiwara, Masatoushi Noumi, and Yasuhiko Yamada, *Geometric aspects of Painlevé equations*, J. Phys. A: Math. Theor. **50** (2017), 073001, DOI 10.1088/1751-8121/50/7/073001.

[16] Masatoushi Noumi and Yasuhiko Yamada, *Affine Weyl Groups, Discrete Dynamical Systems and Painlevé Equations*, Commun. Math. Phys. **199** (1998), 281 – 295, DOI 10.1007/s002200050502.

[17] Michio Jimbo and Hidetaka Sakai, *A q-analog of the sixth Painlevé equation*, Lett. Math. Phys. **38** (1996), 145–154. DOI 10.1007/BF00398316.

[18] P. Painlevé, *Sur les équations différentielles du second ordre et d'ordre supérieur dont l'intégrale générale est uniforme*, Acta Math., **25** (1902), 1-85, DOI 10.1007/BF02419020.

[19] Walter Van Assche, *Discrete Painlevé equations for recurrence coefficients of orthogonal polynomials*, arXiv:math/0512358v2 [math.CA], 2006, 1 - 33.

[20] Walter Van Assche, *Orthogonal polynomials, Toda lattices and Painlevé equations*, Phys. D: Nonlin. Phenom. **434** (2022), 133214, DOI 10.1016/j.physd.2022.133214.

[21] Xuhua He and Sian Nie, *Minimal length elements of extended affine Weyl groups*, Comp. Math. **150** (2014), 1903-1927, DOI 10.1112/S0010437X14007349.